Volume 1 | Number 1 | Jan 2013 | Pages 1–100

Journal of
Materials Chemistry C

Materials for optical and electronic devices
www.rsc.org/materialsC

ROYAL SOCIETY
OF CHEMISTRY

ROYAL SOCIETY
OF CHEMISTRY

www.rsc.org/materialsC

Journal of Materials Chemistry C

ARTICLE TYPE

A Novel Ambipolar Polymer: From Organic Thin-Film Transistors to Enhanced Air-Stable Blue Light Emitting Diodes†

Afsoon Fallahi[a], Faramarz Afshar Taromi[b]*, Alireza Mohebbi[c,d]*, Jonathan D. Yuen[d] and Mohsen Shahinpoor[e]

The search for developing deep blue long-lasting polymer light–emitting diode (PLED) has focused attention on polyfluorene (PFO) keto defect suppression with physical and chemical modifications. This study presents the synthesis and characterization of a new donor-acceptor (DA) polymer, based on
10 naphthalene diimide (NDI) as a strong acceptor and n-phenyl-dithieno[3,2-b:2',3'-d]pyrrole (DTP) as a strong donor. This polymer exhibits ambipolar behavior with stronger n-type properties, 0.07 cm^2 V^{-1} s^{-1}, versus p-type 0.006 cm^2 V^{-1} s^{-1}. By blending PNDIT-alt-DTP into PFO with hole and electron trapping sites, significantly enhanced electroluminescence (EL) efficiency in a simplified polymer light–emitting diode (PLED) was achieved. Further improvement is also achieved by introducing graphene oxide (GO)
15 into the hole injection layer of PEDOT:PSS. A pure and strong long-lasting blue-color in a wide range of bias voltages can be acquired with introducing 5.0wt.% PNDIT-alt-DTP and 0.01wt.% GO. New blend devices have lower turn-on voltages of 3.5 V, compared to 7.0-8.0 V for pure PFO PLEDs, high current efficiency up to 3.8 cd A^{-1} and maximum luminance exceeding 5500 cd m^{-2} which are at least 20 and 60 times greater than pure PFO/0.01GO device, respectively. The enhanced efficiency can be related to
20 improved hole injection and electron blocking nature of GO doped PEDOT:PSS layer as well as reducing singlet exciton quenching at the interface. Additionally, the spatial confinement effect of the ambipolar polymer efficiently enhances the thermal stability of the binary blend and facilitates charge carrier balance and more efficient radiative recombination in the devices. These values are among the highest ever reported for PFO devices doped with an ambipolar polymer working in the air.

25 Keywords: Ambipolar polymer, Graphene oxide (GO), Organic Thin-Film Transistor (OTFT), PLED, Keto-defect suppression

Introduction

Considering the preliminary reports in the field of conjugated electroluminescent polymers, many experimental and theoretical
30 efforts have been implemented to improve the performance of polymer-based light-emitting diodes (PLEDs)[1], solar cells[2] and organic field effect transistors (OFETs).[3] PLEDs have been investigated in both industrial and academic research communities in order to create efficient electroluminescence of
35 the three primary colors, red, green, and blue for thin, flat panel and full color displays.[4,5] Such considerable attention toward PLEDs is due to their unique advantages including light-weight, high resolution, wide color range, rapid response, and low fabrication cost.
40 Besides color adjustment, the main issue in the development of light emitting materials is to increase their quantum efficiency, reduce degradation and light suppression of three primary colors to achieve full color displays. Only red and green organic light emitting diodes (OLEDs) are commercially available as they have
45 shown acceptable efficiencies and lifetimes. For OLEDs in the blue spectral region, many challenges must be solved for improvement in terms of efficiency, air stability and color purity. Among blue light emitting materials, polyfluorene (PFO) is known as a promising conjugated polymer for optoelectronic and
50 electronic applications. They can be used as a host for internal color conversion[6] as well as PLEDs with polarized light emission.[7] However, the desirable electrical and luminescent properties of PFO-based PLEDs are severely deteriorated by the formation of keto-defects, which lead to an additional green low-
55 energy emission band at 2.2–2.3eV, and therefore poor color quality and unsatisfactory lifetimes.[8,9,10,11] Pervious studies show that the green emission of PFO-based conjugated polymers is correlated with thermal oxidation, degradation and crosslinking of PFO.[12,13] Scherf et al have done valuable works to explain PFO
60 structural defects sources and its modeling with quantum-chemical calculations.[14]

Several approaches have been examined to minimize the undesirable long-wavelength emission band and promote photoluminescence (PL) in polyfluorene-based PLEDs.[15,16,17] To adjust the chain conformation structures in PFO, it can be modified chemically by functionalizing side chain moieties, adding end-capping units or long alkyl tails to the C-9 position.[18] A breakthrough for optoelectronic devices based on polymer semiconductors can be the development of doping as a simple strategy. There are different reasons to increase the electroluminescence (EL) efficiency[19] by blending a conductive polymer with other polymeric material. The optimized energy transfer between appropriate partners in a binary blend will improve the quantum yield and facilitate the formation of excitons. More importantly, these defects can trap electrons,[20] holes[21] or excitons[22] and form bound complexes and aggregates, which will become eliminated.[23,24]

Recently, conjugated polymers containing donor-acceptor (DA) backbone architecture demonstrate exceptional advancements in electro-optical devices such as dye-sensitized solar cells (DSSCs), bulk heterojunction (BHJ) solar cells, polymer light-emitting diodes (PLEDs), polymer light-emitting electrochemical cells (PLECs), and OFETs.[25] Additionally, due to their unique properties such as bipolar (electron and hole) charge transport and high solid-state photoluminescence quantum yield,[26,27] they become outstanding candidates to modify and/or optimize characteristics of devices for specific applications.[28] These ambipolar materials can be used in organic light-emitting field-effect transistors (LEFETs)[29] as a serious alternative to OLEDs or as a host which transfers its excitation energy to a luminescent dopant[30] like using novel oxidazole/carbazole hybrid molecule (o-CzOXD), tris-(2,2′-dimethyl-4′-1- phenyl1*H*- benzimidazol-2-yl) biphenyl- 4-yl)yl) biphenyl-4-yl) amine (DM-TIBN), 4,7-dicarbazol-9-yl-[1,10]-phenanthroline (BUPH1), 9,9- bis(9-methylcarbazol-3-yl)- 4,5- diazafluorene (MCAF) and 9,9- bis(9-phenylcarbazaol-3-yl)- 4,5-diazafluorene (PCAF) for red, green and blue electrophosphorescent emitting diodes (PHOLEDs).[31] Zhang et al. reported a promising approach to solution-processed phosphorescent OLEDs with the highest external quantum efficiency of 10.0% and current efficiency of 34.1 cd/A among these hosts.[32] Moreover, DA polymers can be used as emitting layer in PLEDs.[33] For this application, they should meet the requirements of energy level matching for charge carrier injection and acceptance of both holes and electrons with homogeneous thin film formability. It is really important that a DA polymer should balance and stabilize the injected hole and especially electrons in the emissive layer.[34] The electroluminescence of bipolar materials originates from their intramolecular charge transfer (ICT) excited states and intermolecular excimers or exciplexes.[35,51] Jenekhe and his co-workers reported emitting ambipolars with high efficiency up to 7.9 cd/A and 3.0% external quantum efficiency.[36] Fisher et al. reported a simple, single-active-layer ambipolar deep blue OLED with external quantum efficiency up to 4.7%[37] which demonstrates one of the highest efficiencies among handful reports for blue emitters until now.[38] To the best of our knowledge, the influence of a non-fluorescent DA polymer on development of the EL intensity and color purity of PFO-based PLED devices as one of the most important challenges for blue emitters that has not been investigated so far.

In this regard, after synthesizing a novel DA polymer, this paper explains the effect of this novel DA polymer as a dopant on air-stability of PFO-based thin films. Spectrally stable blue PLEDs were analyzed using EL, atomic force microscopy (AFM) and Fourier transform infrared (FTIR) spectroscopies. Our results demonstrated that a single emitting layer containing a tailor-made DA polymer is an efficient and really simple approach to achieve higher charge balance and reduced intermolecular interaction between fluorene moieties. This consequently can suppress exclusive on-chain keto-defect green emission sites. It is believed that beside electron and hole recombination enhancement, the designed blend composition can limit chain mobility due to the high glass transition temperature (T_g) of the DA polymer. This promoted spatial captivity induced exciton stability which consequently overcame the poor spectral strength of blue-emitting polyfluorenes. Recently, doping nanoparticles (NPs) due to their distinctive properties to enhance performance of PLEDs had attracted a lot of researchers.[39] In this paper, we discussed using graphene oxide (GO) into the PEDOT:PSS layer as a modified hole conductive and electron blocking layer. In the PFO blend system with 0.01 wt. % GO in PEDOT:PSS, a maximum luminance of 5500 cd m^{-2} is observed with the Commission Internationale d'Eclairage (CIE) coordinates of (0.1744, 0.1626) at 15 V applied voltage.

Experimental

Instrumentation and materials

All reactions were carried out under nitrogen (Schlenk conditions). All chemicals were obtained from commercial sources and used as received without further purification. UV-vis-NIR spectra were recorded with USB4000-VIS-NIR, Ocean Optics. NMR spectra were recorded on a Bruker DRX-500 and Varian-NMR 600 spectrometers in CDCl$_3$ using TMS as internal standard. Differential scanning calorimetry (DSC) was carried out under nitrogen on a TA Instrument DSC Q10 instrument and also DSC1 star system Mettler Toledo with a scan rate of 5 °C/min. Thermal gravimetric analysis (TGA) was carried out using a TA Instrument TGA Q50 instrument with a heating rate of 10°C/min. Fourier transform infrared (FTIR) spectra were taken with Bruker Tensor 37 Spectrophotometer. Out-of-plane X-ray diffraction (XRD) patterns were obtained with a SmartLab Rigaku X-ray Diffractometer system using Cu Ka source (λ = 1.5418 Å) in air. The thin film samples (~10 nm) for XRD measurements were on the OTS-modified SiO$_2$/Si substrate by drop-casting a polymer solution in chlorobenzene (2 mg mL^{-1}), optionally followed by thermal annealing at 80 °C, 160 °C, 240 °C and 320 °C for 15 min in nitrogen. Gel permeation chromatography (GPC) measurements were performed on a Waters 2615 Separations Module using chloroform + 0.25 % TEA as eluent and polystyrene as standards. Water for all solutions was purified using a Milli-Q water purification system (Millipore, Bedford, MA, USA). Unless otherwise noted, all chemicals were reagent grade and were used without further purification. The PFO used in all the experiments performed here came from a single batch synthesized following the standard literature procedure.[40,41] DSC curve of the synthesized PFO is shown in Figure S5. For PFO, the injection of holes predominates. To increase the efficiency of devices, electron injection has to be significantly boosted.

Therefore, we prepared a DA polymer with more n-type affinity (Schemes S1-S2).

Synthesis of N,N'-Bis(octyldecyl)-2,6-Bis(thiophenyl-5-yl)-1,4,5,8-naphthalene Diimide (2):[42] 2,6-dibromonaphthalene diimide (**1**) (4.4 g, 1.0 mmol), tris(dibenzylideneacetone)dipalladium(0) (30 mg, 0.1 mmol), tris(*o*-tolyl)phosphine (0.040 g, 0.13 mmol) and 2-(tributylstannyl)thiophene (0.450 g, 5.3 mmol) were placed into a double-neck round bottom flask, equipped with a magnet stirrer bar and a reflux condenser. The atmosphere was replaced by argon and the freshly distillated anhydrous THF (60 ml) was added by syringe. The mixture was stirred under reflux overnight, evaporated to dryness and dissolved in boiling isopropanol. An orange solid, precipitated upon cooling, was separated by filtration, washed with cold isopropanol, methanol and dried in vacuo at 40°C. Yield 0.32 g (85%). ^{1}H NMR (500 MHz, CDCl$_3$, δ) = 8.76 (s, 2H), 7.53 (dd, *J* = 5.1, 1.2 Hz, 2H), 7.26 (dd, *J* = 3.6, 0.9 Hz, 2H), 7.20 (m, 2H), 4.07 (d, *J* = 7.2 Hz, 4H), 2.1 (m, 4H), 1.30 (m, 60H), 0.87 (t, *J* = 7.5 Hz, 6H). ^{13}C NMR was not prepared due to low solubility.

Synthesis of N,N'-Bis(octyldecyl)-2,6-bis(5-bromo-thiophenyl-5-yl)-1,4,5,8-naphthalene Diimide (3):[42] Compound **2** (0.310 g, 0.33 mmol) was dissolved in 240 ml of THF. Bromine (0.1 ml, 0.004 mmol) was added under 0°C and the mixture was stirred for 1 hr. The reaction was allowed to warm to room temperature and stirred for 30 min and quenched with sodium thiosulfate. Dark red solid was collected by filtration, washed with MeOH and recrystalized from boiling EtOH . Yield 0.325 g (90%). ^{1}H NMR (500 MHz, CDCl$_3$, δ) = 8.75 (s, 2H), 7.42 (d, *J* = 3.9 Hz, 2H), 7.08 (d, *J* = 3.9 Hz, 2H), 4.08 (d, *J* = 7.3 Hz, 4H), 2.14 (m, 4H), 1.33 (m, 60H), 0.83 (m, *J* = 7.5 Hz, 6H). ^{13}C NMR was not prepared due to low solubility.

Synthesis of 2,6-Bis(tri-methylstannyl)-N-(3,4,5-tris(n-dodecyloxy)phenyl)-dithieno[3,2-b:2',3'-d]pyrrole (5):[43] A deoxygenated solution of N-(3,4,5-tris(n-dodecyloxy)phenyl)-dithieno[3,2-b:2',3'-d]pyrrole (0.51 g, 0.63 mmol) in THF (200 mL) was cooled to –78°C. T-BuLi (2.35 mL, 4.0 mmol, 1.7 M in heptane) solution was added, and the reaction allowed to warm to 0°C and stirred for 1 h, before cooling to –78°C again; Me$_3$SnCl (4.0 mL, 0.4 mmol, 1.0 M in hexane) was then added and the reaction allowed to warm up to room temperature while stirring for 5 h. The reaction was quenched with addition of water and extracted with dichloromethane; the extracts were dried over MgSO$_4$, concentrated under reduced pressure to obtain a pale yellow solid (0.43 g, 60 %). ^{1}HNMR (500 MHz, CD$_2$Cl$_2$, δ): 7.18 (t, J = 7 Hz, 2H), 6.76 (s, 2H), 4.10-3.98 (m, 6H), 1.90-1.80(m, 6H), 1.70-1.12 (72, H), 0.91 (t, J = 7.2 Hz, 9H). ^{13}CNMR (500 MHz, CDCl$_3$, δ): 153.5, 146.7, 135.7 (two peaks), 135.5, 122.1, 119.2, 101.5, 73.7, 69.1, 32.0 (two peaks), 30.5, 29.9, 29.8 (two peaks), 29.5(two peaks), 29.2, 29.1, 29.0, 27.4, 26.3(two peaks), 22.8, 14.3, 13.8, 11.1(5 peaks missing, presumably due to overlap).

Synthesis of PNDIT-alt-DTP: In a Schlenk flask 2,6-Bis(tri-methylstannyl)-N-(3,4,5-tris(n-dodecyloxy)phenyl)-dithieno[3,2-b:2',3'-d]pyrrole (0.090g, 0.082 mmol), **3** (0.093 g, 0.082 mmol) and tris(*o*-tolyl)phosphine (0.020 g, 0.066 mmol) were dissolved in toluene (3 mL). The solution was purged with nitrogen for 30 min and tris(dibenzylideneacetone)dipalladium(0) (5 mg , 0.036

mmol) was added. The reaction was stirred at 100 °C for 1 day. The resulting mixture was poured into a mixture of methanol and 2.0 M HCl (1:1, 300 mL) and stirred overnight. The dark precipitate was filtered, re-dissolved in chloroform and added dropwise to methanol (250 mL). The resulting solid was filtered and subjected to Soxhlet extraction for 3 days successively with methanol, acetone, hexane and cyclohexane for the removal of oligomers and impurities. The remaining polymer was extracted with dichloromethane and precipitated again from methanol, filtered, washed with methanol and dried under vacuum at room temperature. The dark brownish polymer PNDIT-alt-DTP was obtained (0.100 g, 70% yield). M_w/M_n (GPC) = 41730/ 17980 (PDI = 2.3). UV-vis-NIR'.: λ_{max} = 800 nm (in CH$_2$Cl$_2$); 850 nm (thin film). ^{1}H NMR spectrum (Figure S9). Figure S6 shows GPC elution curves and molecular weights of PNDIT-alt-DTP.

Device fabrication materials and methods are explained in the supplementary section.

Results and Discussions
Synthesis and Characterization of Ambipolar Polymer

To synthesize the polymer, a strong donor, dithieno[3,2-b:2',3'-d]pyrrole (DTP) functionalized with a tri-alkoxyphenyl group, and a strong acceptor based on naphthalene tetracarboxylic diimides (NDI)[44] were chosen to enhance the DA interaction and simultaneously produce soluble low band gap polymers for organic electronic applications.[45] NDIs[46] are well-known electron transport materials[47,48] due to their robust nature, flexible molecular-orbital energetics, and excellent charge-transport properties.[49] These low band gap polymers also possess excellent light-fastness and high chemical stability. The DTP unit possesses a large planarity from its rigid, fused ring structure, resulting in the molecule having a low reorganization energy. This can facilitate efficient intermolecular hopping of charge carriers[50] as there is little perturbation of the effective conjugation length.

As illustrated in Scheme 1, PNDIT-alt-DTP was synthesized via Stille copolymerization between 2,6-Bis (2-bromothien-5-yl) naphthalene-1,4,5,8-tetracarboxylic-N,N'-bis (2-octyldodecyl) diimide (**1**) and 2,6-Bis (tri-methylstannyl)-N- (3,4,5-tris (n-dodecyloxy) phenyl)- dithieno [3,2-b:2',3'-d] pyrrole (**2**). The polymer was purified by soxhlet extraction using methanol, acetone, and hexane successively to remove the impurities and oligomers. The remaining crude product in the thimble was then extracted with dichloromethane, and precipitated out by the addition of methanol.

The number average molecular weight (M$_n$) was 18.0 kDa, with a polydispersity index (PDI) of 2.3. The PDI was determined by using gel permeation chromatography (GPC) at room temperature in chloroform against polystyrene standards (Supporting Information, Figure S6). The thermal properties of PNDIT-alt-DTP were examined by thermogravimetric analysis (TGA), which indicated a decomposition temperature of 410 °C under nitrogen (Supporting Information, Figure S7). Differential scanning calorimetry (DSC) shows a first solid-state transition peak at 130 °C, for the first heating scan. (Supporting Information, Figure S8) However, corresponding peak in the subsequent cooling scan was not observed and the two exothermic peaks disappeared in the second heating scan.

Therefore, for annealing the PLED devices we chose the first transition temperature. The optical properties of PNDIT-alt-DTP in chloroform and as a thin film are shown in Figure 1.
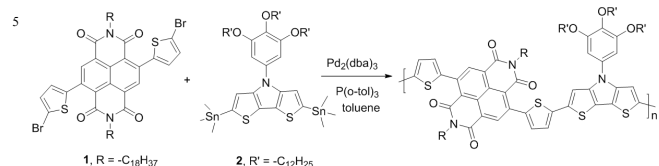
Scheme 1. Synthesis of PNDIT-alt-DTP via Stille-coupling polymerization.

The absorption onset of around 1180 nm in the solid state corresponds to an optical bandgap of 1.05 eV. The electrochemical properties of PNDIT-alt-DTP were investigated by cyclic voltammetry (CV) in order to determine the HOMO and/or LUMO energy levels (Figure S3 in the Supporting Information). The LUMO value of PNDIT-alt-DTP was calculated from the onset reduction potential, which was −3.75 eV, whereas the HOMO value of −4.80 eV was determined from the difference between the LUMO and the optical bandgap.
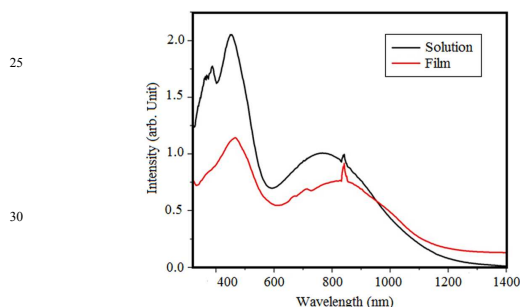

Figure 1. UV-vis-NIR absorption spectra of PNDIT-alt-DTP in CHCl$_3$ solution and thin film on glass substrate.

Thin-film microstructures and morphologies of the present polymers were studied by θ-2θ X-ray diffraction (XRD). As shown in Figure 2, the specular out-of-plane X-ray diffraction pattern for a thin film annealed at 80 °C was essentially featureless. Annealing induced sharpening of a diffraction peak was observed at 2.60 °, corresponding to the (100) reflection of the crystal plane with an interlayer spacing d(100) = 33.95 Å. These observations indicate that the microstructure of the film annealed at 80 °C was kinetically limited and the polymer chains reorganized to ordered lamellar crystalline structures upon annealing. The additional peaks at 240 °C are associated with (200) reflection at 2θ = 4.85 °.
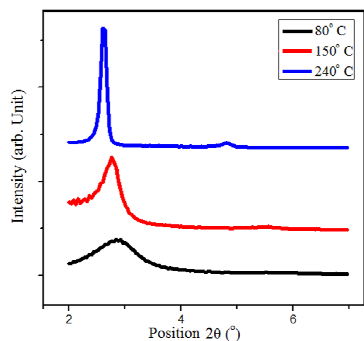

Figure 2. XRD data obtain from drop-cast PNDIT-alt-DTP thin films on octadecyltrichlorosilane (OTS)-modified SiO$_2$/Si substrates annealed at different annealing temperatures.

Fabrication and Measurement of TFT Devices

Bottom-gate, Au bottom-contact transistors were fabricated with PNDIT-alt-DTP as the active layer on heavily doped silicon substrates. The insulator used was a 200 nm SiO$_2$ layer passivated with decyltrichlorosilane (DTS). A more detailed description of the fabrication process is available in the Supplementary section. All of the devices were tested and annealed in nitrogen-purged gloveboxes. Samples measured had channel lengths of 10 μm and channel widths of 1mm. The transfer and output characteristics of a typical PNDIT-alt-DTP transistor, annealed at 150 °C, are shown in Figure 3 with transfer curves in the inset.
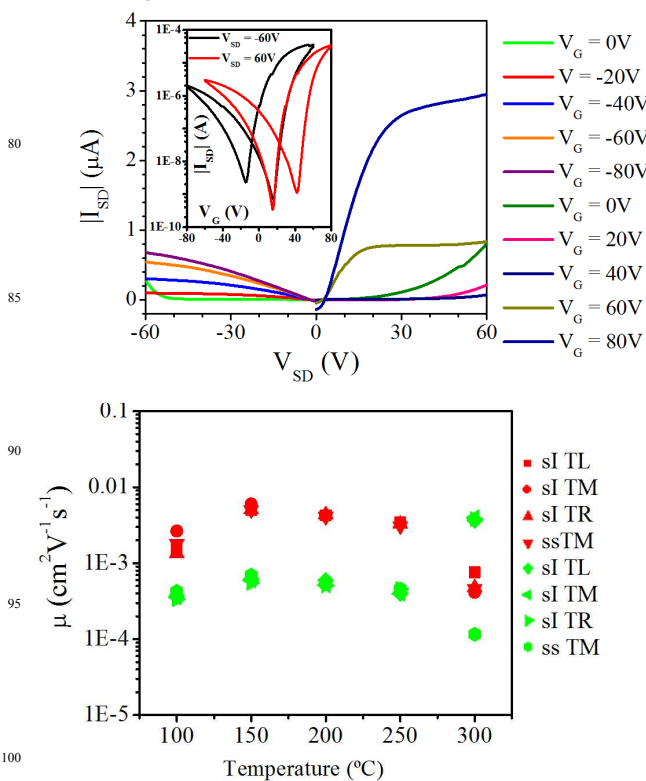

Figure 3. a) Typical transistor output and transfer characteristics of a PNDIT-alt-DTP transistor annealed at 150 °C, with transfer curve in the inset. Mobilities were determined to be 0.07 cm^{2}V^{-1}s^{-1} for n-type transport and 0.006cm^{2}V^{-1}s^{-1} for p-type transport. b) Transistor mobilities as a function of annealing temperature for PNDIT-alt-DTP for n-type transport (red) and p-type transport (green).

The ambipolar behavior can be clearly observed in both the transfer and output characteristics, with stronger n-type properties. In ambipolar thin film transistors (TFTs),[51] transfer curves trace a V-shaped trough with decreasing magnitude of the gate voltage, indicating a transition from unipolar to ambipolar behavior. This is reflected in the output plots exhibiting, at high gate voltages, unipolar transport with standard linear to saturation

current–voltage (*I–V*) transistor characteristics and, at low gate voltages, ambipolar transport with diode-like *I–V* characteristics.

To more accurately quantify and compare device performance, charge-carrier mobilities in the unipolar regimes were calculated with the standard equation used to describe MOS field effect transistors operating in the saturation regime: $I_{DS} = \frac{1}{2}(W/L)\mu C_i(V_G - V_T)^2$, with mobility determined from $\partial|I_{DS}|^{1/2}/\partial V_G$. In order to determine the effect the observed structural ordering has on transport behavior, the transistor samples were annealed at different temperatures. Both n-type and p-type mobilities as a function of annealing temperature are shown on Figure 3, for a set of 4 transistors. The highest average mobility for p-type performance was 0.006 cm^2 V^{-1} s^{-1} at 240 °C and 0.07 cm^2 V^{-1} s^{-1} at 150 °C for n- type.

Fabrication and Measurement of PLED Devices

In this report, we introduce a new approach to improve the poor spectral strength of blue-emitting polyfluorenes and exclude the green emission band by incorporating a DA polymer as a dopant. Figure S1 illustrated the device fabrication method.

Photoluminescence Spectroscopy

Normalized PL emission spectra of pure and blend PFO solution and thin films from chloroform solutions are shown in Figure 4.
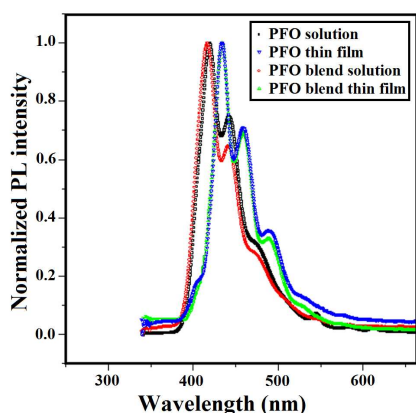

Figure 4. Normalized Fluorescence spectra of pristine PFO solution, spin-cast film annealed at 60°C in air and PFO blend with 5 wt. % PNDIT-alt-DTP.

The observed red-shift by around 20 nm from the solution to the thin film is attributed to aggregate emission in the solid state. The maximum PL spectrum of PFO displays a bathochromic shift about 45 nm with respect to its absorption spectrum, corresponding to a Stokes shift. It exhibits a clear vibronic structure with peaks at about 2.90 (0-0), 2.72 (0-1), and 2.55 (0-2) eV, respectively; a fourth phonon side band (0-3) can also be seen at ~ 2.36 eV. It is clear that the ambipolar polymer as our dopant agent has no photoluminescence in UV-vis region. The only problem in using these materials is their aggregation in high concentration which leads to undesirable red shifts in the PL and EL spectra. Therefore, an optimum concentration of the dopant polymer with PFO to be used in the emissive layer was determined. (Figure S4)

Electroluminescence Spectroscopy

In our first set of experiments, the efficacy of GO as a dopant into the PEDOT:PSS HIL to increase charge carrier performance of the HIL was determined. The EL spectra of our two designed devices (ITO/PEDOT:PSS/PVK/PFO/Al and ITO/PEDOT:PSS:GO/PVK/PFO/Al) are shown in Figure 5.
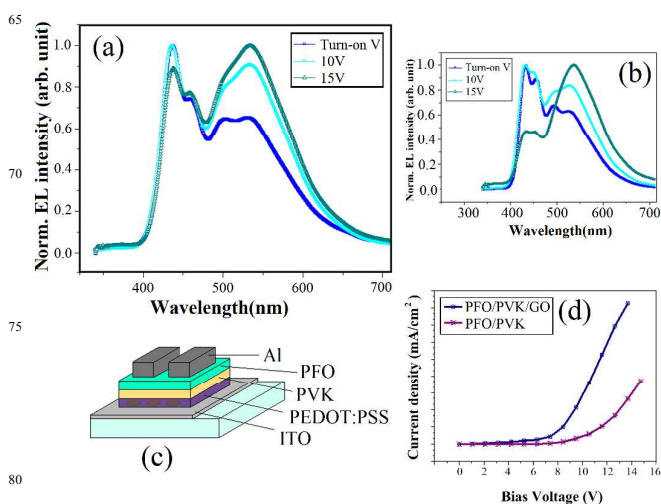

Figure 5. a) Relative EL intensity of device ITO/PEDOT:PSS:GO/PVK/PFO/Al; b) EL intensity of device ITO/PEDOT:PSS/PVK/PFO/Al; c) The cartoon picture shows the device schematic; d) Current density-Voltage (*J-V*) characteristics of these two PLEDs with: pure PEDOT:PSS and blends with GO. All data points used to create the plots were averaged over four trials.

For these devices, blue emission was observed for the first time that a freshly made device was operated even in the air, but the color changed to blue-green and then green-yellowish low-energy emission colors as the operating voltage was increased. It is obvious that hole injection will be enhanced in new devices because of faster charge transfer in the emitting layer. We realized that the green emission delayed and/or moderated with introducing PEDOT:PSS:GO nanocomposite as a new effective hole-injection layer. The turn-on voltages for all devices were around 6.5-7 volts with the surface area of 30mm^2. But these blue PLED devices did not show acceptable life time and color stability.

Figure 5-b shows clearly that the emission from the normal PFO device is reduced gradually by increasing keto defect concentration. As the device is biased at turn-on voltage, the keto emission intensity is only one third of that of the PFO. At 15V bias, the PFO emission is almost entirely quenched and replaced by the broadened green emission. Thus, we can use GO as a tuning factor for PLED devices. All spectra are shown in figure S11 for comparison.

In a follow-up experiment, we designed other devices based on pure PFO and PFO blend with PNDIT-alt-DTP as emitting layer and PEDOT:PSS:GO as the HTL. PFO has high-mobility non-dispersive hole transport but weak and highly dispersive electron transport properties.[52] By incorporating small amounts of a narrow band gap DA polymer with more n-type properties into the emitting layer, great improvement in device performance is

expected due to reduced charge trapping and improved energy transfer mechanisms.[53,54] To begin, three different molar ratios of GO were used to investigate the dependence of film transparency and charge transport, beside device EL properties. Figure 6-b shows the PEDOT:PSS:GO phase alignment after thermal treatment. There are just two phases after adding GO nanoparticles into HIL. GO has a tendency to dissolve in high molecular weight PSS and the nonconductive part of PEDOT:PSS. Hence, it will make the whole system easier to process and increase the conductivity of the water soluble part. Figure 6-d shows the transmittance for pure glass ITO/PEDOT:PSS and the modified substrates with GO.
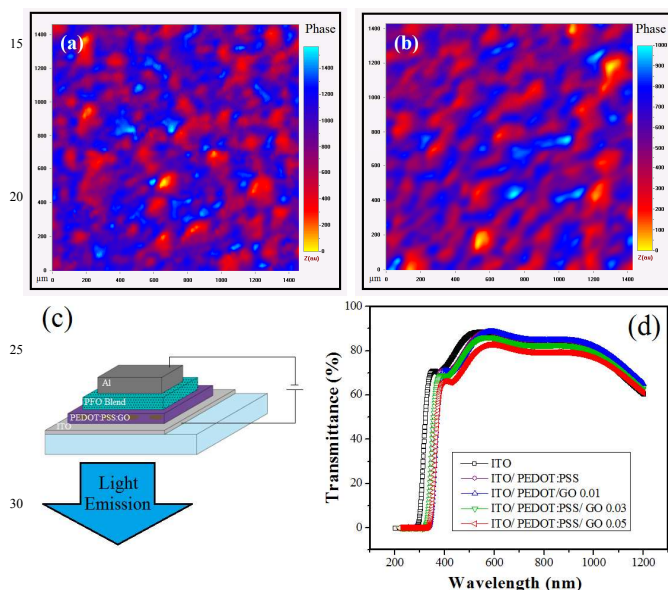

Figure 6. (a) Phase-imaging tapping-mode AFM of PEDOT:PSS:GO composite at room temperature; and (b) Phase alignment after thermal treatment at 120°C (1.4μm x 1.4μm region); (c) Scheme of the PLED device structure and (d) UV-vis spectra for pure and modified HIL. Transmittance for pure ITO (black) and ITO/PEDOT:PSS (purple) and others modified by different percentages of GO.

The room temperature EL spectra of devices with different structures are shown together in Figure 7 for comparison. The EL spectra of pure PFO device without GO was not included in Figure 4 as the EL intensity was too low. The emission of the as-prepared sample consists of a well-resolved structure with typical vibronically structured bands comprising of: one maximum at around 430, a shoulder at around 458, a tail at around 490 nm and an aggregation peak at around 525 nm, assigned to the 0-0, 0-1, 0-2 and 0-3 intrachain singlet transition, with the 0-0 transition being the most intense (exciting wavelength, 380nm). The main characteristic of these peaks is that peak intensity of 0-0 never becomes lower than that of 0-1. It is understood that in Pure PFO devices the intensity ratio of the 0-0 line changes drastically with increasing the GO amount in HIL. But in the blend system, the usual vibronic structure can be observed with the peak intensity decreases as going from the 0-0 line to 0-1, 0-2 and 0-3 lines.
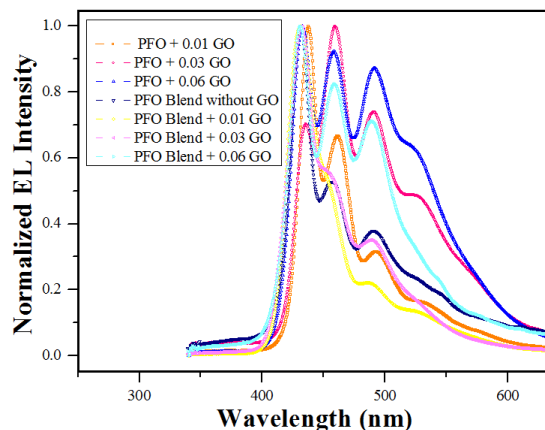

Figure 7. Normalized Electroluminescence of pure PFO PLEDs: ITO/PEDOT:PSS:GO/PFO/Al and PFO blend with 5 wt.% PNDIT-alt-DTP: ITO/PEDOT:PSS:GO/PFO blend/Al. Error bars are 95% confidence intervals for the corrected fluorescence intensity at λ_{max}. All data points used to create the plots were averaged over four trials.

The results revealed that suppression of green emission intensity in the EL spectrum must be related to the enhanced carrier transport in the multicomponent active layer and the modification in the emission pathway. In the blend system, the high n-type property of PNDIT-alt-DTP will enable effective electron injection into the emitting layer (EML), resulting in easier transport of charges in the PFO blend and additional balance between hole and electron injection. This will consequently produce more excitons in the EML. Therefore, a purer and more efficient blue light is emitted from the PFO blend EL device by preventing the formation of keto-defects occurred relative to the pure PFO device.

The other obvious feature in these spectra is that in devices without the DA polymer, red shifts up to 7nm of the spectra can be observed. From the electronic perspective, we can conclude that the DA polymer has a tendency to balance the hole and electron injection in the system. The DA polymer also can eliminate the excimer interface state formation and peak transitions by creating better hole and electron paths in the EML (Figures S12 and S13).

It is also noticeable that the concentration of GO influence the emission bands shoulders. As illustrated in EL spectra in figure 7, it can be recognized that with just 0.01 wt.% GO, we have a purer blue color with anomalous EL enhancement. In these devices, 0.01 wt. % was high enough to show a stable and high intensity blue color emission even in 15V. The turn-on voltages for these PFO and PFO blend devices (with surface areas of 6×7 mm^2) were 7-8 and 3.5-5 volts, respectively. For the blend systems, the turn-on voltages were substantially decreased than PFO and even PFO/PVK PLED devices[55] (Figures S1 and S2).

Atomic Force Microscopy

Previous reports have indicated that the morphology of the polymer films used for PLEDs is critical for the performance and lifetimes.[56] Film morphology and the polymer/electrode interface properties can be altered by heat treatment, bringing about an enhancement of the device performance.[57] Height and phase AFM

images were taken in un-annealed and annealed samples, as shown in Figure 8. Annealing modified the film morphology by smoothing the surface topography due to lower granularity and increasing the thermal resistance of the polymer blend.[58]
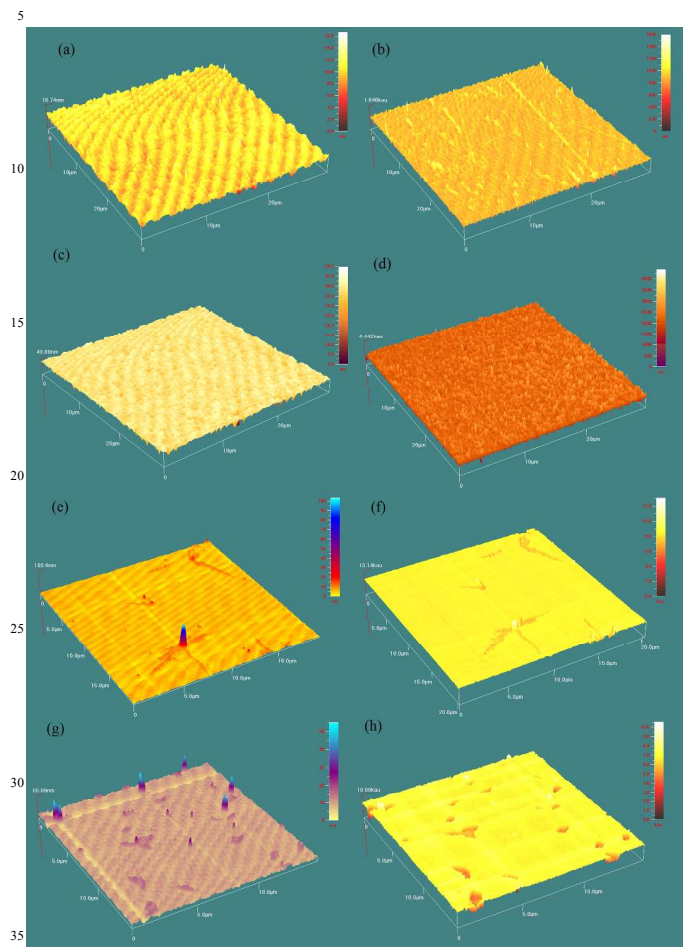

Figure 8. AFM surface topography (Left) and corresponding phase (Right) images of pristine PFO (a-d) and PFO/PNDIT-alt-DTP containing 95:5 wt.% copolymer (e-f) thin films : (a), (b), (e) and (f) for as spun film and (c), (d), (g) and (h) for films annealed at 120 °C. Note that PNDIT-alt-DTP chains are molecularly dispersed in the PFO matrix due to the low content.

Before annealing, long PNDIT-alt-DTP chains probably twist, tangle with each other, and aggregate into big particles. Results show an obvious roughness with the root mean square (rms) of 3.906 nm (Figure 8e and 8f). After annealing at 120°C, the tangled chains become separated through the melting and stretching of the blend, giving rise to film smoothness with reduced rms of 2.047 nm. Lowering the surface roughness of the thin film will decrease the leakage current of the corresponding PLED devices and limits the PFO chain mobility. Subsequently, the device lifetime increases.

As shown in Figure 8, the blend film exhibits unique morphological feature from aggregated rod-like (e, f) (in room temperature) to plate-like (g, h) (at 120 °C) morphology. We believe this change in film morphology is responsible for its better charge carrier mobility and less keto-defect formation.[59] In

addition, the self-segregation of these well-dispersed chains can provide a kinetic barrier to the diffusion of ambient oxidants such as oxygen, moisture, and ozone into the bulk.[60,61]
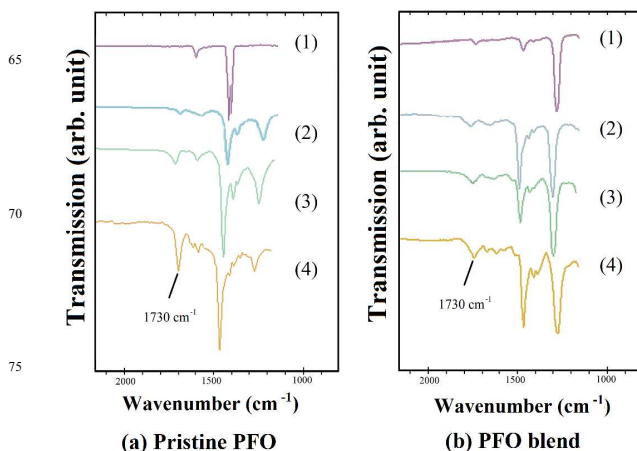

Figure 9. FTIR spectra of polymer films. a) PFO film, b) PFO/PNDIT-alt-DTP containing 95:5 wt. % blend film, before (1) and after annealing in the oven of 40°C for 5 min (2), 30 min (3), and 60 min (4). The >C=O stretching mode at ~1730 cm^{-1} is changed in (a) but is almost unchanged in (b). All data points used to create the plots were averaged over four trials.

Infrared Spectroscopy

Chemical changes resulting from thermo-oxidative degradation during film preparation are examined by Fourier transform infrared (FTIR) spectroscopy. Figure 9 shows the FTIR spectra of pristine PFO and its blend with PFO/PNDIT-alt-DTP copolymer as cast and after thermal annealing in the air atmosphere with the different annealing times. The most obvious changes in the IR spectra of degraded samples are observed in the carbonyl stretch region of an aromatics ketone (~1700 cm^{-1}). When both films were annealed for 5, 30, and 60 min, the carbonyl stretching peak gradually increased for pristine PFO at 1737 cm^{-1} as evidence of thermo-oxidation, while blend samples did not show same phenomena. Noted that small carbonyl stretching peaks at IR spectra of blend film might originate from the PNDIT-alt-DTP copolymer since, it has already carbonyl bonds in its molecular structure. These results showed that a desirable long-term stability of PFO PLED cells can be resulted by using our DA copolymer as dopant. Molecular interaction between PFO main chain and dopant polymer may protect the C-9 position in the fluorene units from formation of keto-defects as low-energy trapping sites for singlet excitons which will decrease trapped charges in its electroluminescence.[12]

PLED Device Characterization

Based on the *J-V* characteristics of PFO blend PLED shown in Figure 10, lower driving voltages of ~ 3.5V was observed versus pure PFO PLED with ~ 6V. However, with increasing applied voltage, a significant increase in current density of PFO blend PLEDs observed which was much faster than those of pure PFO PLEDs. For instance, the driving voltage at a current density of 60 mA cm^{-2} is 8.6 V for PFO blend PLED while for PFO PLED

is 14.5 V. Also, the pure PEDOT:PSS in PFOPLED showed the lowest *J-V* curve. On the other hand, the device with the highest doping concentration of graphene, 0.06 wt. %, in PFO blend PLED had the highest *J-V* slope. It also exhibited the tendency of *J-V* curve to increase with GO concentration because the conductivity of the HIL was augmented by adding GO as dopant.
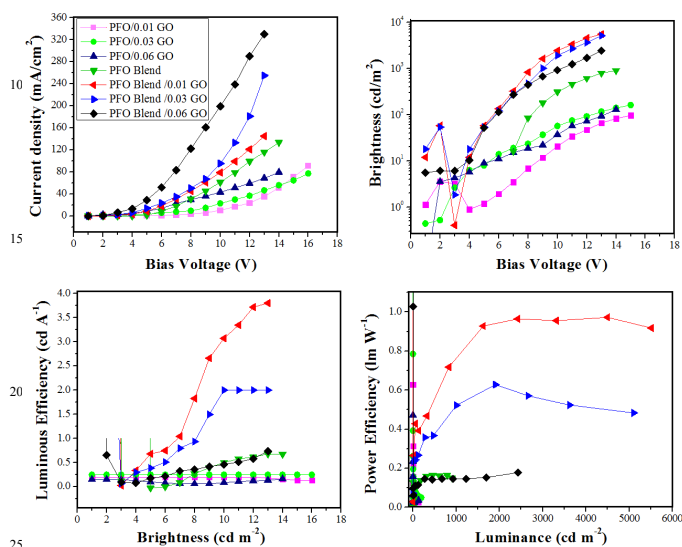

Figure 10. a) *J-V* curves for the systems with the configuration of ITO/PEDOT:PSS:GO/PFO: PNDIT-alt-DTP /Al. and ITO/ PEDOT:PSS:GO/PFO/Al having various graphene concentrations of 0.01, 0.03, and 0.06 wt.%. b) voltage–luminescence (V–L) characteristics of PLEDs of the polymer blends. c, d) Efficiencies of PLEDs of the polymers with the above mentioned configurations; (c) Current density-Luminance efficiency (cd/A), and (d) Current density-Power efficiency (lm/W). All data points used to create the plots were averaged over four trials.

The key feature is that the currents passing through the blend devices are much higher than through the pure PFO device, suggesting that there is better charge transfer and hole accumulation in the blends. In comparison, we have a mild growth gradient for all *J-V* curves of devices without DA polymer. The results for all the devices are summarized in Table 1. The PFO blend devices with GO doped PEDOT:PSS layer work noticeably better than the reference devices or without GO in terms of turn-on voltage, luminance, and current efficiency. For example, in PFO blend device with 0.01 wt.% GO, the turn-on voltage is reduced to 3.5 V, and the maximum luminance has a significant enhancement of more than 60 times which is pretty superior for a PFO device works in the air. This improved brightness is created by doping PNDIT-alt-DTP into the emitting layer. As a result of increasing electron and hole transporting abilities by introduction of the GO and PNDIT-alt-DTP moieties, the efficiencies are boosted more than 19 times. We can deduce that the hole injection is improved by the GO, based on the current–voltage characteristics. GO doped PEDOT:PSS layer can create a blocking layer against singlet exciton quenching as well as improving hole injection and electron-blocking. These findings imply that the carriers are confined into the EML after an efficient injection, resulting in high exciton formation efficiencies even in high current densities. The huge discrepancies between the performances of the blend and pure PFO devices further confirm the advantage of our newly prepared ambipolar material.

Table 1. Summary of device performance with different emitting and HI layers.

Active layer	HIL (PEDOT: PSS + wt.%GO)	0-0 Peak emission (nm)	Turn-on voltage (V)	Current Density (mA/cm^2)	Luminance$_{Max}$[a] (cd m^{-2})	Current efficiency$_{max}$[b] (cd A^{-1})	Power efficiency (lm W^{-1})
PFO	0	0	0	0	0	0	0
PFO	0.01	437	6.5	90.88	97	0.20	0.05
PFO	0.03	435	7	77.17	161	0.25	0.06
PFO	0.06	433	7	79.3	129	0.16	0.03
PFO blend	0	430	6	133.64	901	0.68	0.16
PFO blend	0.01	430	3.9	145	5510	3.8	0.97
PFO blend	0.03	430	4.5	255	5100	2	0.52
PFO blend	0.06	431	3.5	330	2430	0.73	0.15

[a] Maximum brightness

[b] Maximum luminescence efficiency

Using x, y as the coordinates (reported in the supplementary section in Table S1), a two-dimensional chromaticity diagram (the CIE 1931 color space diagram) can be plotted as shown in Figure 11. The purity of blue color is enhanced after blending with our novel DA polymer, especially with lower percentages of GO (0.03, 0.01 wt. %). Those are in the blue region close to pure PFO solution fluorescence. This pure and long lasting deep blue emission is a promising feature for RGB PLEDs. The highest intensity of pure blue for present work was in optimized PEDOT:PSS:GO (0.01 wt. %) hole transport layer with blended PFO.
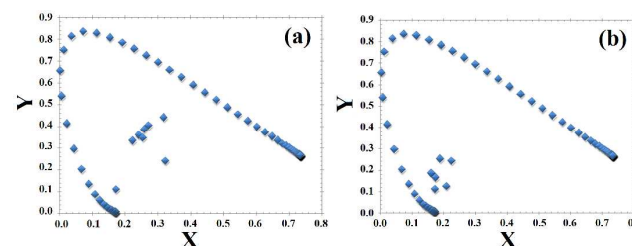

Figure 11. Comparison between pure (a) and blend (b) PFO devices CIE chromaticity.

Our PFO device had very low luminescence efficiency that was not detectable with our Luminance Meter. But based on other reported maximum luminescence for pure PFO devices,[62] a significant increase in the maximum luminance of 5500 cd m^{-2} is observed in the PFO blend system with 0.01 wt. % GO. Thus, the simple addition of the novel DA polymer can not only stabilize the blue emission of the PLED, but also enhance its brightness and durability. This work can encourage researchers to design new DA molecules with electronic structures that optimize electron and hole injection properties to allow further improvement in PLED devices; especially for those that contain polymers with electrically-induced structural defects, allowing them to have more fluorescence permanence and efficiency.

Conclusions

In conclusion, we have successfully used polyfluorene, which has a keto-defect prone structure with low spectral-stability, and blended it with a novel high mobility ambipolar charge transport polymer, PNDIT-alt-DTP. Based on chromaticity diagram data, our binary blend devices produced a substantially less red-shifted, purer and stronger blue color with improved thermal stability. Due to the chain mobility inhibiting nature of our reported polymer, the 2.2-2.4 eV emission bands of fluorenone defects and bipolarons were hindered and the blue emission was stabilized even during operating in air. Our novel results strongly indicate that adjusting the DA properties of the synthesized polymer can offer better charge mobilities within the active layer and lower driving-voltages. Also the intensity of these emissive layers can be increased by utilization of convenient conductors in both sides of active layer. As a simple strategy, GO is a promising material to use in HIL to maximize hole injection, abridge OLED layers by eliminating HTL and allow more efficient hole-electron recombination within the emissive layer. Electrons can be blocked and singlet exciton quenching can be reduced by this new HIL resulting in more efficient radiative recombination between holes and electrons inside the emitting layer. This results in higher currents observed in blend devices compared to the pure PFO devices, leading to better emission properties. We believe this strategy is both simple and effective, and should be explored at a much greater scale.

Acknowledgements

Abbreviations

GO, Graphene oxide; OTFT, Organic Thin-Film Transistor; PLED, Polymer light emitting diode; PFO, polyfluorene; DA,donor-acceptor; EL, electroluminescence; PL, plotoluminescence; CV, cyclic voltame-try.

Notes and references

a,b Department of Polymer Engineering and Color Technology, Amirkabir University of Technology (Tehran Polytechnic), 424 Hafez Avenue, P.O. Box 15875-4413, Tehran, Iran
E-mail: *afshar@aut.ac.ir*
c Department of Chemistry and Biochemistry, University of California Santa Barbara, Santa Barbara, CA 93106, USA
Email: *ali.mohebbi@polyera.com*
d Center for Polymers and Organic Solids University of California Santa Barbara, CA 93106, USA
e Department of Mechanical Engineering, University of Maine, Orono, ME 04469-5711, USA

†*Electronic Supplementary Information (ESI) available: [Device fabrication methods, CV, DSC, TGA, NMR, Synthesis schemes]. See DOI: 10.1039/b000000x/*

1 a) D. Y. Kim, H. N. Cho, and C. Y. Kim, *Prog. Polym. Sci.* **2000**, *25*, 1089; b) L. Akcelrud, *Prog. Polym. Sci.* **2003**, *28*, 875; c) L. S. Hung, C. H. Chen, *Mater. Sci. Eng.* **2002**, *R 39*, 143.

2 a) G. Yu, J. Gao, J. C. Hummelen, F. Wudl, A. J. Heeger, Science **1995**, 270, 1789; b) E. Bundgaard, F. C. Krebs, Sol. Energy Mater. Sol. Cells, **2007**, *91*, 954; C) B. C. Thompson, J. M. J. Fre´chet, Angew. Chem. Int. Ed. **2008**, *47*, 58; d) S. Gunes, H. Neugebauer, N. S. Saricitci, Chem. Rev. **2007**, *107*, 1324; E) K. M. Coakley, M. D. McGehee, Chem. Mater. **2004**, *16*, 4533.

3 a) H. Sirringhaus, N. Tessler, R. H. Friend, *Science* **1998**, *280*, 1741; b) L. L. Chua, J.-F. Chang, J. Zaumseil, E. C. W. Ou, P. K. H. Ho, H. Sirringhaus, R. H. Friend, *Nature* **2005**, *434*, 194; c) I. McCulloch, M. Heeney, C. Bailey, K. Genevicius, I. Macdonald, M. Shkunov , D. Sparrowe, S. Tierney, R. Wagner, W. M. Zhang, M. L. Chabinyc, R. J. Kline, M. D. McGehee, M. F. Toney, *N at. Mater.* **2006**, *5*, 328.

4 a) R. Friend, R. Gymer, A. Holmes, J. Burroughes, R. Marks, C. Taliani, D. Bradley, D. Dos Santos, J. L. Brédas, M. Lögdlund, W. R. Salaneck *Nature.* **1999**, *397*, 121; b) M. T. Bernius, M. Inbasekaran, J. O'Brien, W. Wu, *Adv. Mater.* **2000**, *12*, 1737. c) A. Kraft, A. C. Grimsdale, A. B. Holmes, *Angew. Chem., Int. Ed.* **1998**, *37*, 402; d) A. J. Heeger, , *Solid State Commun.* **1998**, *107*, 673.

5 a) I. Sokolik, Z. Yang, F. E. Karasz, D. C. Morton, *J. Appl. Phys.* **1993**, *74*, 3584; b) Z. Peng, Z. Bao, M. E. Galvin, *Chem. Mater.* **1998**, *10*, 2086; c) C. J. Tonzola, M. M. Alam, S. A. Jenekhe, *Adv. Mater.* **2002**, *14*, 1086; d) D. Neher, *Macromol. Rapid Commun.* **2001**, *22*, 1365.

6 a) T. Virgili, D. G. Lidzey, D. D. C. Bradley, *Adv. Mater.* **2000**, *12*, 58; b) P. A. Lane, L. C. Palilis, D. F. O'Brien, C. Giebeler, A. J. Cadby, D. G. Lidzey, A. L. Campbell, W. Blau, D. D. C. Bradley, *Phys. Rev. B* **2001**, *63*, 235206.

7 a) M. Grell, W. Knoll, D. Lupo, A. Meisel, T. Miteva, D. Neher, H. G. Nothofer, U. Scherf, A. Yasuda, *Adv. Mater.* **1999**, *11*, 671; b) E. J. List, R. Guentner, P. Scanducci de Freitas, U. Scherf, , *Adv. Mater.* **2002**, *14*, 374.

8 a) E. J. List, M. Gaal, R. Guentner, P. S. de Freitas, U. Scherf, , *Synth. Met.* **2003**, *139*, 759; b) H. Wiesenhofer, D. Beljonne, G. D. Scholes, E. Hennebicq, J. L. Brédas, E. Zojer, , *Adv. Funct. Mater.* **2005**, *15*, 155.

9 I. Franco, S. Tretiak, *Chem. Phys. Lett.* **2003**, *372*, 403.

10 W. Beenken, M. Sun, G. Zhao, T. Pullerits, *Phys. Status Solidi B.* **2008**, *245*, 849.

11 a) M. M. Mandoc, B. de Boer, P. W. M. Blom, *Phys. Rev. B* **2006**, *73*, 155205; b) J. Cornil, J. L. Brédas, J. Zaumseil, H. Sirringhaus, *Adv. Mater.* **2007**, *19*, 1791; c) R. Steyrleuthner, S. Bange, D. Neher, *J. Appl. Phys.* **2009**, *105*, 8; d) C. R. McNeill, N. C. Greenham, *Appl. Phys. Lett.* **2008**, *93*, 3.

12 W. Zhao, T. Cao, J. M. White, *Adv. Funct. Mater.* **2004**, *14*, 783.

13 Y. Noh, D. Kim, O. Dong, B. Gu, Y. Yoshida, K. Yase, B. Jung, E. Lim, H. Shim, R. Azumi, *Appl. Phys. Lett.* **2004**, *85*, 4.

14 a) X. H. Yang, F. Jaiser, D. Neher, P. V. Lawson, J. L. Brédas, E. Zojer, R. Güntner, P. S. de Freitas, M. Forster, U. Scherf, *Adv. Funct. Mater.* **2004**, *14*, 1097; b)E. Zojer, A. Pogantsch, E. Hennebicq, D. Beljonne, J-L Brédas, P. S. de Freitas, U. Scherf, E. JW. List, J. Chem. Phys. **2002**, *117*, 6794; c) L. Romaner, A. Pogantsch, P. S. de Freitas, U. Scherf, M. Gaal, E. Zojer, E. JW. List. *Adv. Func. Mater.* **2003**, *13*, 597.

15 W. L. Yu, J. Pei, W. Huang, A. J. Heeger, *Adv. Mater.* **2000**, *12*, 828.

16 a) F. Wu, D. S. Reddy, C. Shu, M. S. Liu, A. K. Jen, *Chem. Mater.* **2003**, *15*, 269; b) D. Katsis, Y. H. Geng, J. J. Ou, S. W. Culligan, A. Trajkovska, S. H. Chen, L. J. Rothberg, *Chem. Mater.* **2002**, *14*, 1332.

17 K. Hosoi, T. Mori, T. Mizutani, T. Yamamoto, N. Kitamura, *Thin Solid Films.* **2003**, *438*, 201.

18 a) C. H. Chou, S. L. Hsu, K. Dinakaran, M. Y. Chiu, K. H. Wei, *Macromolecules* **2005**, *38*, 745; b) S. F.Lim, R. H. Friend, I. D.

Rees, J. Li, Y. Ma, K. Robinson, A. B. Holmes, E. Hennebicq, D. Beljonne, F. Cacialli, *Adv. Funct. Mater.* **2005**, *15*, 981; c) X. Chen, J. L. Liao, Y. Liang, M. O. Ahmed, H. E. Tseng, S. A. Chen, *J. Am. Chem. Soc.* **2003**, *125*, 636; d) M. C. Hung, J. L. Liao, S. A. Chen, S. H. Chen, A.C. Su, *J. Am. Chem. Soc.* **2005**, *127*, 14576.

19 A. Pron, P. Rannou, *Prog. Polym. Sci.* **2002**, *27*, 135; b) X. Zhang, D. M. Kale, S. A. Jenekhe, *Macromolecules* **2002**, *35*, 382.

20 Z. Zhao, J. H. Li, P. Lu, Y. Yang, *Adv. Funct. Mater.* **2007**, *17*, 2203.

21 X. Xu, Y. Zhao, E. J. Sie, Y. Lu, B. Liu, S. A. Ekahana, X. Ju, *ACS Nano*, **2011**, *5*, 3660.

22 a) H. Yersin, in *Transition Metal and Rare Earth Compounds*, Springer Berlin Heidelberg, 2004, 1-26; b) V. Jankus, C. Winscom, A. P. Monkman, *Adv. Funct. Mater.* **2011**, *21*, 2522.

23 J. R. Tozoni, F. E. G. Guimaraes, T. D. Z. Atvars, B. Nowacki, L. Akcelrud, T. J. Bonagamba, *Eur. Polym. J.* **2009**, *45*, 2467.

24 G. Meng, S. Velayudham, A. Smith, R. Luck, and H. Liu, *Macromolecules* **2009**, *42*, 1995.

25 a) J. H. Seo, E. B. Namdas, A. Gutacker, A. J. Heeger, G. C. Bazan, *Adv. Funct. Mater.* **2011**, *21*, 3667; b) E. J. Meijer, D. M. de Leeuw, S. Setayesh, E. Van Veenendaal, E. E. Huisaman, P. W. M. Blom, J. C. Hummelen, U. Scherf, T. M. Klapwijk, *Nat. Mater.* **2003**, *2*, 678; c) C. S. Sangeeth, P. Stadler, S. Schaur, N. S. Sariciftci, R. Menon, *J. Appl. Phys.* **2010**, *108*, 113703; d) Y. Hyashi, H. Kanamori, I. Yamada, A. Takasu, S. Takagi, K. Kaneko, *Appl. Phys. Lett.* **2005**, *86*, 052104.

26 A. Duarte, K. Pu, B. Liu, G.C. Bazan, *Chem. Mater.* **2011**, *23*, 501.

27 S. A. Choulis, Y. Kim, J. Nelson, and D. D. C. Bradley, *Appl. Phys. Lett.* **2004**, *85*, 3890.

28 a) L. Burgi, M. Turbiez, R. Pfeiffer, F. Bienewald, H. J. Kirner, C. Winnewisser, *Adv. Mater.* **2008**, *20*, 2217; b) G. Horowitz, *Adv. Mater.* **1998**, *10*, 365; c) H. E. Katz, Z. Bao, *J. Phys. Chem. B* **2000**, *104*, 671; d) C. D. Dimitrakopoulos, P. R. L. Malenfant, *Adv. Mater.* **2002**, *14*, 99; e) S.-Y. Takizawa, V. A. Montes, P. Anzenbacher, Jr., *Chem. Mater.,***2009***, 21*, 2452.

29 M. C. Gwinner, D. Kabra, J. L. Roberts,T. J. Brenner, B. H. Wallikewitz, C. R. McNeill, R. H. Friend, H. Sirringhaus, *Adv. Mater.* **2012**, *24*, 2728.

30 D. Kim, V. Coropceanu, J. L. Brédas, *J. Am. Chem. Soc.* **2011**, *133*, 17895.

31 a) Y. T. Tao,Q. Wang, C. L. Yang, Z. Q. Zhang, T. T. Zou, J. G. Qin, D. G. Ma, *Angew. Chem. Int. Ed.* **2008**, *47*, 8104; b) Z. Y. Ge, T. Hayakawa, S. Ando, M. Ueda, T. Akiike, H. Miyamoto,T. Kajita, M. A. Kakimoto, *Adv. Funct. Mater.* **2008**, *18*,584; c) Z. Q. Gao, M. Luo, X. H. Sun, H. L. Tam, M. S. Wong, B. X. Mi, P. F. Xia, K. W. Cheah, C. H. Chen, *Adv. Mater.* **2009**, *21*, 688; e) C. J. Zheng, J. Ye, M. F. Lo, M. K. Fung, X. M. Ou, X. H. Zhang, C. S. Lee, *Chem. Mater.* **2012**, *24*, 643-650; f) Y. Zhang, W. Haske, D. Cai, S. Barlow, B. Kippelen, S. R. Marder, *RSC Adv.* **2013**, *3*, 23514.

32 Y. Zhang, C. Zuniga, S. J. Kim, D. Cai, S. Barlow, S. Salman, V. Coropceanu, J. L. Brédas, B. Kippelen, S. Marder, *Chem. Mater.* **2011***, 23*, 4002.

33 J. M. Hancock, A. P. Gifford, Y. Zhu, Y. Lou, S. A. Jenekhe, *Chem. Mater.* **2006,** *18,* 4924.

34 K. R. Justin Thomas, M. Velusamy, J. T. Lin, C. H. Chuen, Y. T. Tao, *Chem. Mater.* **2005,** *17*, 1860.

35 a) W. Chunwaschirasiri, B. Tanto, D. Huber, M. Winokur, *Phys. Rev. Lett.* **2005***, 94*, 107402; b) H. Lu, C. Liu, T. Jen, J. Liao, H. Tseng, C. Huang, M. Hung, S. Chen, *, Macromolecules* **2005***, 38*, 10829; c) Y. LIN, T. -L. YE, YU CHEN, D. -G. MA, Z. -K. CHEN, Y. -F. DAI, Y. -X. LI, *J. Polym. Sci., Part A: Polym. Chem.*, **2010**, *48*, 5930.

36 J. M. Hancock, A. P. Gifford, Y. Zhu, Y., Lou, S. A. Jenekhe, *Chem. Mater.* **2006**, *18*, 4924.

37 A. L. Fisher, K. E. Linton, K. T. Kamtekar, C. Pearson, M. R. Bryce, M. C. Petty, *Chem. Mater.* **2011**, *23*, 1640.

38 a) Y. Yang, P. Cohn, A. L. Dyer, S.-H. Eom, J. R. Reynolds, R. K. Castellano, J. Xue, *Chem. Mater.* **2010**, *22*, 3580; b) T.-C. Tsai, W.-Y. Hung, L.-C. Chi, K.-T. Wong, C.-C. Hseih, P.-T. Chou, *Org. Electron.* **2009**, *10*, 158.

39 a) B. Riedel, Y. Shen ,J. Hauss ,M. Aichholz ,X. Tang ,U. Lemmer ,M. Gerken*, Adv. Mater.* **2011***, 23,* 740; b) N. Sakai, G. K. Prasad, Y. Ebina, K. Takada, T. Sasaki, *Chem. Mater.*, **2006**, *18*, 3596; c) N.G. Semaltianos S. Logothetidis, N. Hastas, W. Perrie, S. Romani, R. J. Potter, G. Dearden, K.G. Watkins, P. French, M. Sharp, *Chem. Phys. Lett.* **2010**, *484*, 283; d) J. Zhang, L. Gao, J. Sun, Y. Liu, Y. Wang, J. Wang, *Diam. Relat. Mater.* **2012**, *22*, 82; e) H. S. Woo, R. Czerw, S. Webster, D. L. Carroll, *Appl. Phys. Lett.* **2000**, *77*, 1393; f) F. Xu, W. Q. Zhu, L. Yan, H. Xu, L. H. Xiong, J. H. Li, *Org. Electron.* **2012**, *13*, 302; g) S. Shi, V. Sadhu, R. Moubah, G. Schmerber, Q. Bao, S. R. P. Silva, *J. Mater. Chem. C,* **2013**, *1,* 1708.

40 M. Ranger, D. Rondeau, and M. Leclerc, *Macromolecules* **1997,** *30,* 7686.

41 N. Miyaura, A. Suzuki, *Chem. Rev.* **1995** , *95*, 2457.

42 C. Gu, W. Hu, J. Yao, H. Fu, *Chem. Mater.* **2013**, *25*, 2178.

43 T.T. Steckler, X. Zhang, J. Hwang, R. Honeyager, S. Ohira, X. -H. Zhang, A. Grant, S. Ellinger, S.A. Odom, D. Sweat, *J. Am. Chem. Soc.* **2009**, *131*, 2824.

44 J.D. Yuen, F. Wudl, *Energy Environ. Sci.* **2013**, *6*, 392.

45 a) J. Liu, R. Zhang, G. Sauvé, T. Kowalewski, R. D. McCullough, *J. Am. Chem. Soc.* **2008**, *130*, 13167; b) T. T. Steckler, X. Zhang, J. Hwang, R. Honeyager, S. Ohira, X.-H. Zhang, A. Grant, S. Ellinger, S. A. Odom, D. Sweat, *J. Am. Chem. Soc.* **2009**, *131*, 2824.

46 J. H. Oh, S.–L. Suraru, W.-Y. Lee, M. Konemann, H. W. Hoffken, C. Roger, R. Schmidt, Y. Chung, W.-C. Chen, F. Wurthner, Z. Bao, *Adv. Funct. Mater.* **2010**, *20*, 2148.

47 C. Ego, D. Marsitzky, S. Becker, J. Zhang, A. C. Grimsdale, K. Müllen, J. D. MacKenzie, C. Silva, R. H. Friend, *, J. Am. Chem. Soc.* **2003***, 125*, 437.

48 A. Babel, Y. Zhu, K. Cheng, W. Chen, S. A. Jenekhe, *, Adv. Funct. Mater.* **2007***, 17*, 2542.

49 Y. Wen, Y. Liu, C.-A. Di, Y. Wang, X. Sun, Y. Guo, J. Zheng, W. Wu, S. Ye, G. Yu, *Adv. Mater.* **2009**, *21*, 1631.

50 a) W. Zhang, J. Li, L. Zou, B. Zhang, J. Qin, Z. Lu, Y. F. Poon, M. B. Chan-Park, C. M. Li, *Macromolecules* **2008**, *41*, 8953; b) J. Liu, R. Zhang, G. Sauvé, T. Kowalewski, R. D. McCullough, *J. Am. Chem. Soc.* **2008**, *130*, 13167.

51 a) A. R. Mohebbi, J. Yuen, J. Fan, C. Munoz, R. S. Shirazi, J. Seifter and F. Wudl, *Adv. Mater.* **2011**, *23*, 4644; b) J. Fan, J. D. Yuen, W. Cui, J. Seifter, A. R. Mohebbi, M. Wang, H. Zhou, A. Heeger and F. Wudl, *Adv. Mater.* **2012**, *24*, 6164; c) J. Fan, J. D. Yuen, M. Wang, J. Seifter, J. H. Seo, A. R. Mohebbi, D. Zakhidov, A. Heeger, F. Wudl, *Adv. Mater.* **2012**, *24*, 2186; d) A. N. Aleshin, I. P. Shcherbakov, V. N. Petrov, A. N. Titkov, *Org. Electron.* **2011**, *12*, 1285.

52 a) M. Redecker, D. Bradley, M. Inbasekaran and E. Woo, *Appl. Phys. Lett.* **1998**, *73*, 1565; b) A. J. Campbell, D. D. Bradley, H. Antoniadis, *Appl. Phys. Lett.* **2001**, *79*, 2133.

53 C. Zhong, C. Duan, F. Huang, H. Wu, Y. Cao, *Chem. Mater.* **2011**, *23*, 326.

54 Y. Liao, C. Lin, K. Wong, T. Hou, W. Hung, *Org. Lett.* **2007,** *9*, 4511.

55 S. T. Huang, D. J. Liaw, L. G. Hsieh, C. C. Chang, M. K. Leung, K. L. Wang, W. T. Chen, K. R. Lee, J. Y. Lai and L. H. Chan, *J. Polym. Sci., Part A: Polym. Chem.*, **2009**, *47*, 6231.

56 X. Yang, A. Alexeev, M. A. Michels, J. Loos, *Macromolecules* **2005**, *38*, 4289.

57 a) S. Z. Chen, S. H. Peng, T. Y. Ting, P. S. Wu, C. H. Lin, C. Y. Chang, J. J. Shyue, J. H. Jou, *Appl. Phys. Lett.* **2012**, *101*,

153304; b) G. E. Jabbour, R. Radspinner and N. Peyghambarian, *Selected Topics in Quantum Electronics, IEEE Journal of*, **2001**, *7*, 769.

58 a) A. P. Kulkarni, S. A. Jenekhe, *Macromolecules* **2003,** *36,* 5285; b) V. N. Bliznyuk, S. A. Carter, J. C. Scott, G. Klarner, R. D. Miller, D. C. Miller, *Macromolecules* **1999**, *32*, 361.

59 a) B. A. Jones, A. Facchetti, M. R. Wasielewski, T. J. Marks, *J. Am. Chem. Soc.* **2007**, *129*, 15259; b) R. Schmidt, J. H. Oh, Y.-S. Sun, M. Deppisch, A.-M. Krause, K. Radacki, H. Braunschweig, M. Konemann, P. Erk, Z. Bao, F. Wurthner, *J. Am. Chem. Soc.* **2009**, *131*, 6215.

60 B. A. Jones, M. J. Ahrens, M. H. Yoon, A. Facchetti, T. J. Marks, M. R. Wasielewski, *Angew. Chem. Int. Ed.* **2004**, *43*, 6363.

61 J. H. Oh, Y.-S. Sun, R. Schmidt, M. F. Toney, D. Nordlund, M. Konemann, F. Wu¨rthner, Z. Bao, *Chem. Mater.* **2009**, *21*, 5508.

62 X. Gong, P.K. Iyer, D. Moses, G.C. Bazan, A. J. Heeger, S.S. Xiao, *Adv. Funct. Mater.* **2003**, *13*, 325.